Letter

Plasma Stark effect of He II Paschen-α: Resolution of the disagreement between experiment and theory

Franciszek Sobczuk[*] and Krzysztof Dzierżęga[†]
Marian Smoluchowski Institute of Physics, Jagiellonian University, ul. Łojasiewicza 11, 30-348 Kraków, Poland

Evgeny Stambulchik[‡]
Faculty of Physics, Weizmann Institute of Science, Rehovot 7610001, Israel

(Received 17 June 2022; accepted 2 August 2022; published 22 August 2022)

There is a significant disagreement between the experimental and theoretical plasma Stark shift of the hydrogenlike helium Paschen-α line ($\lambda = 468.568$ nm). Here, it is demonstrated that the controversy can be resolved by accounting for the plasma polarization shift and other related effects arising from the charged plasma particles penetrating the wave-function extent of the bound electron. For experimental verification, a laser-induced helium plasma with $n_e = 1.50 \times 10^{24}$ m^{-3} and $T_e = 68\,200$ K, as independently determined by using the Thomson scattering method, was studied. Excellent agreement is observed between the theoretical and experimental line width and line shift, and more generally, for the entire line shape.

DOI: 10.1103/PhysRevE.106.L023202

I. INTRODUCTION

Hydrogenlike atoms are the simplest and best understood one-electron atomic systems and indeed the first ones to which the quantum description—first of the "old" Bohr theory [1], then modern quantum mechanics [2]—was applied and tested against. A quantum mechanical explanation of the Stark effect in hydrogenlike atoms followed immediately [3].

However, the plasma-caused Stark broadening [4] is a rather complex phenomenon, and even for hydrogenlike transitions it remains a topic of active research [5]. In particular, there is a significant disagreement between the experimental and theoretical plasma Stark shift of the He II Paschen-α line (a transition between levels with the principal quantum number $n = 4$ and $n = 3$) [6]. Unfortunately, there is also a similar scatter between the results of different experiments [6–12].

The experimental determination of the Stark shift is one of the most difficult measurements, requiring high experimental precision, including wavelength calibration and appropriate data processing procedures. Otherwise, the accuracy quoted, as in the above-mentioned studies, is usually a few dozen percent. Furthermore, the shift depends almost linearly on the plasma free-electron density n_e which must be obtained independently [13]; evidently, the uncertainty in this parameter (usually $\gtrsim$10%) adds to the total error bars. These significant experimental uncertainties make comparisons with theoretical results debatable.

In a recent study [6], it was suggested to analyze the shift-width relation instead of the shift and width separately as a function of the plasma density. This approach eliminates the explicit dependence on n_e and the associated uncertainties from the consideration and, by choosing a sufficiently dilute "reference" plasma, avoids the need for absolute wavelength calibration. Within the error bars, the results agreed with some previous studies [10,11] and allowed testing theoretical results plotted on the same "shift-width" graph. The comparison indicated that the calculations significantly, by ~40%, underestimated the shift.

Here, it is shown that the disagreement can be resolved by accounting for the plasma polarization shift (PPS) [14] and other related effects arising from penetrating collisions. Although the importance of PPS for He II Paschen-α was understood long ago [15], the effect has been calculated so far outside the line-broadening framework, often based on statistical considerations; not surprisingly, there is a wide divergence in the PPS values given by different authors (see Ref. [10] and references therein). Instead, the present calculations are performed using line-shape computer simulations (CSs) [16] treating ions and electrons on an equal footing, recently modified to account for the full Coulomb interaction between the radiator and the plasma perturbers [17]. The calculations are verified against new data obtained in a dedicated benchmark experiment with a laser-induced plasma well characterized using the Thomson scattering (TS) method.

II. EXPERIMENT

The experimental setup is shown schematically in Fig. 1. A vacuum chamber is evacuated below 10^{-5} mbar and then filled with pure helium at 1500 mbar. The plasma is created in the center of the chamber by tightly focusing second-harmonic ($\lambda = 532$ nm) Q-switched Nd:YAG laser pulses (4.5 ns duration, 115 mJ energy, and 10 Hz repetition rate) with a 75-mm focal length aspheric lens. For plasma

[*]franciszek.sobczuk@doctoral.uj.edu.pl
[†]krzysztof.dzierzega@uj.edu.pl
[‡]evgeny.stambulchik@weizmann.ac.il

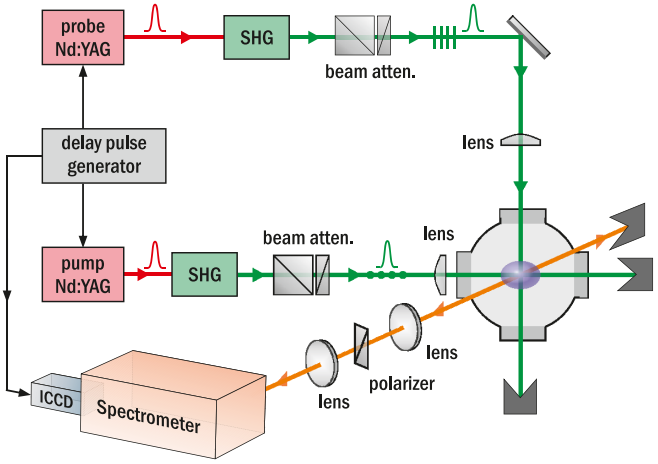

FIG. 1. Experimental setup.

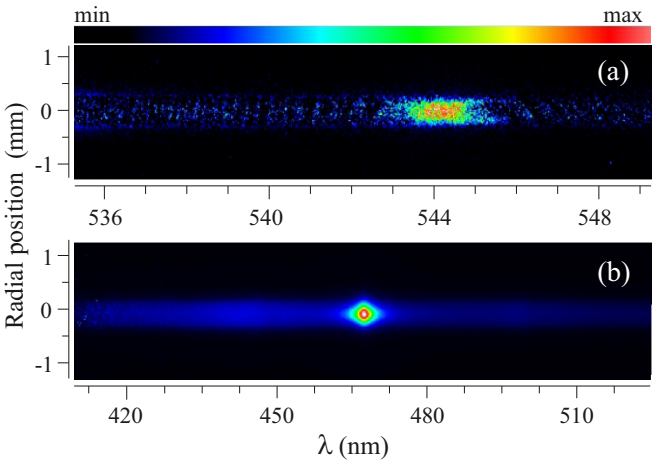

FIG. 2. Images of laser scattering (LS) spectrum obtained with the probe laser at 532 nm (a), and of plasma emission with the He II Paschen-α spectral line recorded for a delay of 40 ns between the pump and probe laser pulses (b).

diagnostics using the Thomson scattering method, another second-harmonic single-mode (<0.5 pm spectral width, 6 ns duration, and 10 Hz repetition rate) Nd:YAG laser is used. To avoid heating the plasma by the laser pulse in the inverse bremsstrahlung process, its energy is attenuated to 5 mJ using a Rochon prism polarizer and a half-wave plate. This probe laser beam, focused at a spot of about 100 μm in diameter in the plasma volume, propagates orthogonally to the one creating the plasma, henceforth called the pump beam, and is polarized perpendicularly to the direction of observation. The delay between the two laser pulses is controlled by a digital delay pulse generator with an accuracy better than 200 ps.

Plasma radiation and laser scattering (LS) light are observed perpendicularly to the laser beams by imaging the investigated plasma region onto the entrance slit of a Czerny-Turner spectrometer (750 mm focal length) equipped with a gated two-dimensional intensified charge-coupled device (ICCD). Instrumental profiles are determined using different cw laser sources and are well approximated by a pseudo-Voigt function with a full width at half maximum (FWHM) of 0.30 nm ($\approx$14 cm^{-1}). The spectral sensitivity of the optical and detection systems is determined with a calibrated halogen lamp. Special attention is paid to wavelength calibration. For this purpose, atomic He and Xe spectral lines, appearing in the spectral range that covers the studied line He II Paschen-α, are used. These lines are observed in a laser-induced plasma created in the same chamber in the He-Xe mixture at atmospheric pressure and at late stages of its evolution. The uncertainty of the wavelengths, determined in this way, is 0.03 nm.

Optical signals are recorded 40 ns after plasma initiation with an ICCD gate width as short as 5 ns and averaged over 15 000 laser shots. The short gate width brings the studied plasma closer to the quasistationary state and increases the signal-to-noise ratio of the LS light as well. The latter is also improved by insertion of the polarizer into the path of measured light.

Images of the measured LS and plasma emission spectra, corrected for the spectral sensitivity of the experimental system and with the CCD dark-current and plasma continuum background subtracted, are shown in Fig. 2. The LS spectra have a high spatial resolution, limited only by the size of the probe laser beam in the interaction area, whereas the emission spectra are laterally integrated and require an inverse Abel transform to recover the radially resolved spectra corresponding to the LS ones. Because of the high electron number density and, consequently, the high plasma frequency, only the redshifted part of the TS electron feature is recorded.

III. THEORETICAL MODEL

Briefly, the Coulomb radiator-plasma interaction for a one-electron radiator with nucleus charge Z_N is approximated by a Debye-screened potential

$$V_{RP} = \sum_\sigma Z_\sigma \sum_{p\in\sigma} \left(\frac{Z_N e^{-\kappa_\sigma r}}{r_p} - \frac{e^{-\kappa_\sigma |\vec{r}_a - \vec{r}_p|}}{|\vec{r}_a - \vec{r}_p|} \right) \equiv V_{\rm net} + V_I, \tag{1}$$

with $V_{\rm net}$ the interaction of the plasma with the net radiator charge,

$$V_{\rm net} = (Z_N - 1) \sum_\sigma Z_\sigma \sum_{p\in\sigma} \frac{e^{-\kappa_\sigma r}}{r_p}, \tag{2}$$

and V_I the interaction with the internal states of the radiator,

$$V_I = \sum_\sigma Z_\sigma \sum_{p\in\sigma} u(\vec{r}_a, \vec{r}_p; \kappa_\sigma), \tag{3}$$

where

$$u(\vec{r}_a, \vec{r}_p; \kappa) = \frac{e^{-\kappa r_p}}{r_p} - \frac{e^{-\kappa |\vec{r}_a - \vec{r}_p|}}{|\vec{r}_a - \vec{r}_p|}. \tag{4}$$

These expressions account for different inverse screening Debye lengths κ_σ for different plasma species σ with charge Z_σ. $\vec{r}_a$ and $\vec{r}_p$ are positions of the bound electron and the pth perturber, respectively.

$V_{\rm net}$ governs the dynamics of plasma particles in molecular-dynamics (MD) simulations based on the velocity Verlet algorithm [18], and results in a time series of $V_I(t)$ according to Eq. (3). Coulomb interactions between plasma particles

are accounted by the effective potential, Eq. (1). Such "trivial" MD simulations provide accurate results for weakly to moderately coupled plasmas [19]. $V_{\rm net}$ causes some electrons to move along closed orbits, resulting in the thermodynamically sound electron radial distribution function [17]. For the line-shape calculations, however, these classically "bound" electrons are excluded during the initial MD seeding. Instead, a correct ion charge-state balance is enforced by including singly and doubly ionized He atoms in the proportion given by a collisional-radiative model [20].

The evolution of the radiator dipole operator is obtained by solving the Heisenberg equation

$$-i\hbar\frac{\partial}{\partial t}\vec{d}(t) = [H(t), \vec{d}(t)], \tag{5}$$

with the time-dependent Hamiltonian

$$H(t) = H_0 + V_I(t), \tag{6}$$

where H_0 is the Hamiltonian of the unperturbed radiator. Finally, the line shape is given by

$$I(\omega) \propto \sum_{if}\langle|\vec{d}_{fi}(\omega)|^2\rangle, \tag{7}$$

where $\vec{d}(\omega)$ is the Fourier transform of $\vec{d}(t)$, the sums are over the initial and final states i and f, respectively, and the plasma average denoted by the angle brackets is accomplished by averaging over CS runs.

The principal improvement of these calculations as compared, for example, to those from Ref. [6], is the evaluation of the matrix elements of Eq. (4) *exactly*, in particular, preserving the monopole interaction. This is contrary to the "standard" multipole expansion, which assumes $r_a \ll r$ and $r_a\kappa \ll 1$, and begins with the dipole term. This exact treatment is applied to all perturbers with $r < R_{\rm exact} = 3\times10^{-7}$ cm and the usual multipole expansion, including the long-debated $\propto\vec{\nabla}\cdot\vec{F}$ term [21], outside of this range. The $R_{\rm exact}$ chosen exceeds the typical r_a of the $n = 4$ states by an order of magnitude, ensuring a good numerical match of the two approaches at the $r = R_{\rm exact}$ boundary.

There are two contributions to the line shift: the nonlinear Stark effect due to the Stark mixing between states with different principal quantum numbers n (so-called "quenching" collisions) and nondipole (mainly monopole and quadrupole) interactions between the bound electron of the radiator and the charged plasma particles. The first contribution was already taken into account in the calculations presented in Ref. [6].

Each of the contributions is computationally heavy; simultaneously accounting for both of them results in computational complexity of the next order, making such calculations impractical. Instead, the two contributions are calculated separately and combined assuming additivity of shifts and widths (see Sec. V for a discussion). This approach is demonstrated in Fig. 3. Base calculations are the "standard" (without penetration effects) dipole approximation within the pure degenerate atomic model, i.e., without coupling between bound electron states with different n's. This results in a fully symmetric line shape with zero shift. Lifting the assumption of a degenerate model yields a broader and shifted asymmetric profile. For these calculations, all states with $3 \leqslant n \leqslant 6$ were included in the Hamiltonian. Based on the analysis performed earlier [6], it is estimated that the omission of levels with $n < 3$ and $n > 6$ introduced a minor uncertainty (∼5%) in the shift and even a smaller uncertainty (2%–3%) in the width.

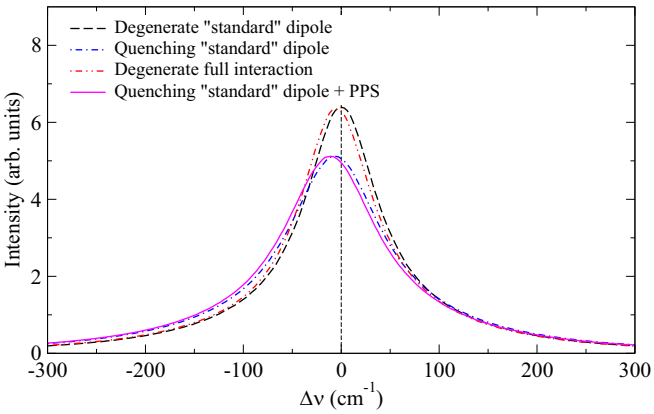

FIG. 3. He II Paschen-α shape calculated under various assumptions. The plasma parameters assumed are those experimentally determined based on the TS diagnostics: $n_e = 1.50\times10^{24}$ m^{-3} and $T = 68\,200$ K.

On the other hand, keeping the degenerate-model assumption while using the full interaction results in a shifted line shape, mainly due to the PPS. In particular, the width increases almost negligibly (<1%) due to the cancellation of various effects [17,22]. There is also practically no asymmetry. This allows one to construct the final line shape by applying this shift to the line shape obtained by quenching the "standard" dipole approximation.

IV. RESULTS

The plasma parameters n_e and T_e were determined by fitting the spectral density function, convolved with the instrumental profile, to the measured redshifted electron feature of the TS spectrum. It is worth mentioning that unlike, e.g., optical emission spectroscopy, the results do not depend on assumptions about the plasma thermodynamic equilibrium, its chemical composition, or a selected plasma model, as is the case in the line profile calculations. Details on the Thomson scattering technique and its application to the study of laser-induced plasma and plasma Stark broadening of spectral lines can be found in Refs. [23–27]. In the case of the plasma studied, the complete analysis takes into account the distribution of n_e resulting from some plasma inhomogeneity, its evolution over the measured interval, and a shot-to-shot variability. These effects were included in the fitted function assuming that n_e is subject to a normal distribution. At the same time, variations of T_e are neglected, assuming their minor impact on TS signals. The values of n_e and T_e obtained in this way amount to $1.50(17)\times10^{24}$ m^{-3} and 68 200 K (5.88 eV), respectively, with the fit shown in Fig. 4.

The respective He II Paschen-α line profile is determined by applying the inverse Abel transformation to the measured chordal intensity distribution. This spectrum is then fit by a sum of a Lorentzian and a linear function, with the latter representing the plasma continuum and the far wings of

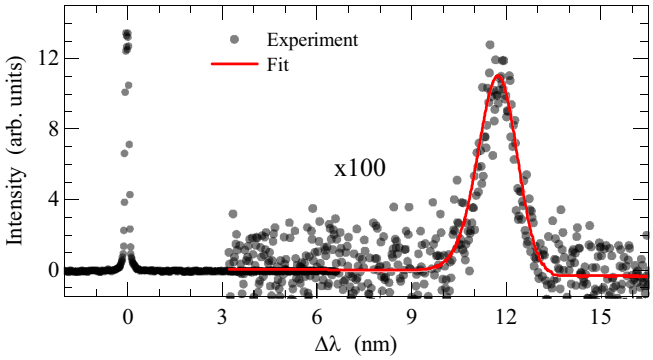

FIG. 4. A TS spectrum recorded at a delay of 40 ns on the plasma axis with the probe laser of 532 nm (solid gray circles). The solid line represents the theoretical model of the spectral density function. The electron number density and temperature determined from the fit are $1.50(17) \times 10^{24}$ m^{-3} and 68 200 K, respectively. The LS signal at the probe wavelength ($\Delta\lambda = 0$) due to the Thomson and Rayleigh scattering is shown for comparison.

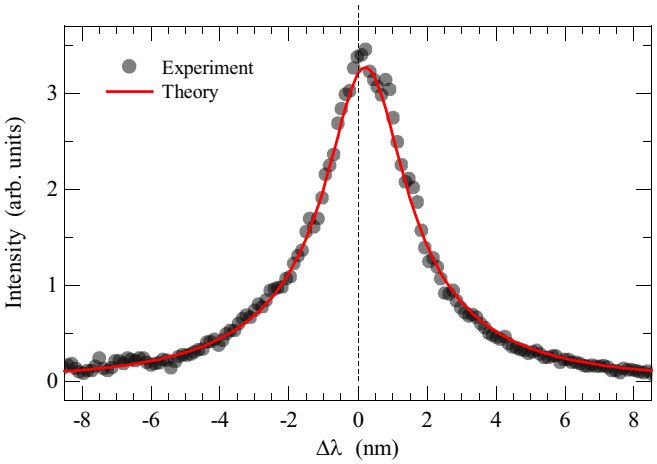

FIG. 6. A comparison of the experimental line shape and the theoretical one, convolved with the instrumental function and the Doppler broadening.

neighboring spectral lines. Finally, this linear function is subtracted from the original experimental spectrum, leaving only the He II Paschen-α shape (see Fig. 6) with the width (FWHM) and the shift determined to be 3.09(2) and 0.23(3) nm, respectively. Taking into account instrumental broadening and negligibly small (0.044 nm) Doppler broadening, the Stark width in this case is 2.78(2) nm.

TS analysis indicates a Gaussian-like distribution of n_e, resulting from either some plasma inhomogeneity or its evolution over the measurement interval (or both). Consequently, the theoretical line shape is obtained by averaging several line shapes calculated for different values of n_e with an additional weighting factor proportional to the intensity of the Paschen-α transition. To infer the latter, a collisional-radiative model is used [20], assuming a steady-state plasma. The resulting density dependencies are shown in Fig. 5. It is seen that the Stark width and shift are indeed approximately $\propto n_e^{2/3}$ and $\propto n_e$,

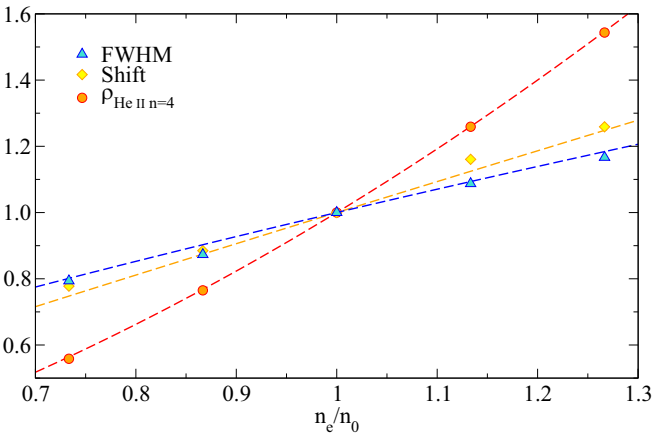

FIG. 5. Density dependencies of the He II Paschen-α plasma Stark width and shift and the population of its upper level. The lines are power-law best fits, with the exponents of 0.71, 0.94, and 1.85, respectively. All quantities are normalized to their values at $n_0 = 1.50 \times 10^{24}$ m^{-3}.

respectively [6], while the population of the upper level and, hence, the line intensity is close to $\propto n_e^2$ (see, e.g., Ref. [28]). Eventually, the influence of the density distribution turns out to be very minor due to the rather narrow distribution of n_e with a standard deviation of approximately 10%.

The width and shift of the resulting theoretical profile are 125 and -11.4 cm^{-1}, respectively (2.76 and 0.250 nm in wavelength units). The uncertainties in the width and shift values are 5% and 15%, respectively (see Sec. V for some details).

The experimental and theoretical line shapes are given in Fig. 6. As seen from the comparison, the agreement is very good.

V. DISCUSSION

The improvement in the line-shape calculations gained by using the full-interaction Hamiltonian is demonstrated in Fig. 7, where experimental data from recent measurements [6] in a pinch plasma setup are also shown. Since no independent plasma diagnostics was implemented in that study, a shift-width parametric graph (with n_e as an independent parameter in the case of the theoretical curves) is made. Specifically, the shift d versus the FWHM w raised to the power of 3/2 is plotted. With the width and shift dependence on n_e being approximately $\propto n_e$ and $\propto n_e^{2/3}$, respectively, nearly linear resulting plots are obtained. It is clearly seen that the dipole approximation with the penetration effects neglected underestimates the shift significantly, whereas the full-interaction calculations describe the experimental results very well. Note that the theoretical curves in the figure are calculated for $T = 4$ eV, according to the assumption made in Ref. [6]. It is rather plausible, however, that in pinch plasmas higher densities correspond to higher temperatures, with the plasma polarization shift decreasing. This may explain the minor, but apparently systematic, deviation of the rightmost (i.e., corresponding to the highest densities) experimental points from the theoretical curve.

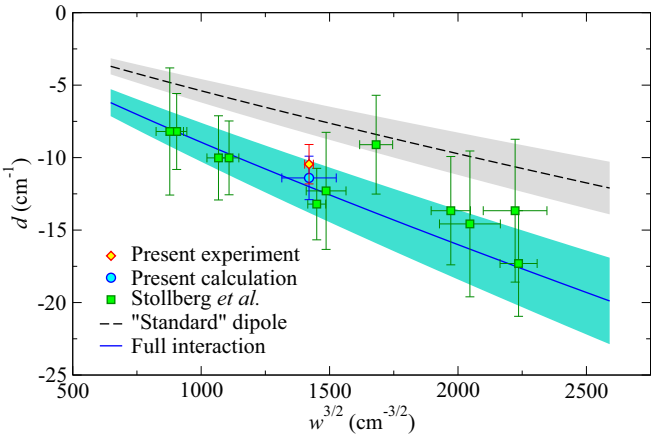

FIG. 7. The shift-width graph with experimental data from the present and previous (Stollberg *et al.* [6]) studies and theoretical calculations. The "standard"-dipole and full-interaction curves are obtained assuming $T = 4$ eV, with the shaded areas designating the theoretical uncertainties.

In order to assess the accuracy of the theoretical approximation used (assuming that the PPS and the quadratic Stark shift are additive), calculations were performed keeping only the $n = 3$ and $n = 4$ states in the Hamiltonian. With such a limited basis, a full calculation, including the quenching terms, becomes doable. A comparison of this calculation with the approximate one shows that the latter overestimates the total shift by about 1 cm^{-1}. This value constitutes a major contribution to the inaccuracy of the calculated shift: First, the $\langle n = 3|V_I|n = 4\rangle$ coupling contributes to both the upper and lower levels of the transition, acting in the opposite direction, that is, any associated inaccuracy is doubled. On the other hand, the Stark shifts of the upper and lower levels due to any other state, e.g., with $n = 5$, have the same sign and cancel to some extent, and the higher n, the cancellation is stronger.

The other principal approximation is separation of the total interaction V_{RP} into $V_{\rm net}$ and V_I [see Eqs. (1)–(3)], inherent for all semiclassical models of plasma line-shape broadening [29,30], analytical and computer simulations alike. Although well justified in the case of the "standard" multipole calculations of line broadening of degenerate, hydrogenlike radiators, for penetrating collisions, this approximation introduces a minor inaccuracy [17]: As a charged perturber penetrates the wave function of the bound electron, its motion is governed by the monopole interaction with an effective $Z^*(r)$ ($Z_N < Z^* < Z_N + 1$), rather than Z_N. Evidently, this correction affects electrons and ions in the opposite directions, further enhancing plasma polarization in the vicinity of the nucleus and increasing the PPS. Thus, this approximation slightly underestimates the shift.

Therefore, the two main sources of the inaccuracy—the assumption about additivity of the Stark shift due to the quenching and penetrating collisions, and variation of the effective core charge close to the nucleus—are minor and, furthermore, partially cancel. The total uncertainty in the calculated shift is believed to be 1.5 cm^{-1} ($\approx$0.03 nm in the wavelength units).

VI. CONCLUSIONS

In order to resolve a significant discrepancy between the theoretical and experimental plasma Stark shift of the Paschen-α line in hydrogenlike helium, calculations are performed, in which the interaction between the radiating atom and the plasma is evaluated without relying on the multipole approximation, taking into account penetration of the plasma particles into the wave-function extent of the bound electron. The calculations are compared to measurements in a laser-induced plasma, which is accurately diagnosed using Thomson scattering. The experimental and theoretical line shapes compare very well, highlighting the importance of nondipole, in particular, monopole, radiator-plasma interaction terms for reliable calculations of the plasma Stark shift of spectral lines in hydrogenlike ions.

ACKNOWLEDGMENTS

The authors thank Carlos A. Iglesias for valuable comments on the manuscript. F.S. acknowledges a partial support of his work by the National Science Centre (Poland) Grant No. 2019/33/N/ST2/02823. The work of E.S. is supported in part by the Israel Science Foundation (Grant No. 1426/17).

[1] N. Bohr, London, Edinburgh Dublin Philos. Mag. J. Sci. **26**, 1 (1913).
[2] E. Schrödinger, Ann. Phys. **384**, 361 (1926).
[3] P. S. Epstein, Phys. Rev. **28**, 695 (1926).
[4] H. R. Griem, *Spectral Line Broadening by Plasmas* (Academic, New York, 1974).
[5] A. V. Demura, Atoms **6**, 33 (2018).
[6] C. Stollberg, E. Stambulchik, B. Duan, M. A. Gigosos, D. G. Herrero, C. A. Iglesias, and C. Mossé, Atoms **6**, 23 (2018).
[7] C. Fleurier and P. L. Gall, J. Phys. B: At. Mol. Phys. **17**, 4311 (1984).
[8] T. L. Pittman and C. Fleurier, Phys. Rev. A **33**, 1291 (1986).
[9] R. Kobilarov, M. V. Popović, and N. Konjević, Phys. Rev. A **37**, 1021 (1988).
[10] A. Gawron, J. D. Hey, X. J. Xu, and H.-J. Kunze, Phys. Rev. A **40**, 7150 (1989).
[11] S. Büscher, S. Glenzer, T. Wrubel, and H.-J. Kunze, J. Phys. B: At., Mol. Opt. Phys. **29**, 4107 (1996).
[12] R. J. Peláez, C. Pérez, V. R. González, F. Rodríguez, J. A. Aparicio, and S. Mar, J. Phys. B: At., Mol. Opt. Phys. **38**, 2505 (2005).
[13] There is also a temperature dependence, but it is much weaker.
[14] G. C. Junkel, M. A. Gunderson, C. F. Hooper, and D. A. Haynes, Phys. Rev. E **62**, 5584 (2000).
[15] H. R. Griem, Phys. Rev. A **38**, 2943 (1988).

[16] E. Stambulchik and Y. Maron, J. Quant. Spectrosc. Radiat. Transfer **99**, 730 (2006).
[17] E. Stambulchik and C. A. Iglesias, Phys. Rev. E **105**, 055210 (2022).
[18] L. Verlet, Phys. Rev. **159**, 98 (1967).
[19] E. Stambulchik, D. V. Fisher, Y. Maron, H. R. Griem, and S. Alexiou, High Energy Density Phys. **3**, 272 (2007).
[20] Yu. V. Ralchenko and Y. Maron, J. Quant. Spectrosc. Radiat. Transfer **71**, 609 (2001).
[21] C. A. Iglesias, High Energy Density Phys. **38**, 100921 (2021).
[22] L. A. Woltz and C. F. Hooper, Phys. Rev. A **30**, 468 (1984).
[23] O. E. Evans and J. Katzenstein, Rep. Prog. Phys. **32**, 207 (1969).
[24] D. H. Froula, S. H. Glenzer, N. C. Luhmann, and J. Sheffield, *Plasma Scattering of Electromagnetic Radiation: Theory and Measurement Techniques* (Academic, New York, 2011).
[25] K. Dzierżęga, A. Mendys, and B. Pokrzywka, Spectrochim. Acta, Part B **98**, 76 (2014).
[26] K. Dzierżęga, T. Pięta, W. Zawadzki, E. Stambulchik, M. Gavrilović-Božović, S. Jovićević, and B. Pokrzywka, Plasma Sources Sci. Technol. **27**, 025013 (2018).
[27] K. Dzierżęga, F. Sobczuk, E. Stambulchik, and B. Pokrzywka, Phys. Rev. E **103**, 063207 (2021).
[28] E. Kroupp, E. Stambulchik, A. Starobinets, D. Osin, V. I. Fisher, D. Alumot, Y. Maron, S. Davidovits, N. J. Fisch, and A. Fruchtman, Phys. Rev. E **97**, 013202 (2018).
[29] M. A. Gigosos, J. Phys. D: Appl. Phys. **47**, 343001 (2014).
[30] T. A. Gomez, T. Nagayama, P. B. Cho, D. P. Kilcrease, C. J. Fontes, and M. C. Zammit, J. Phys. B: At., Mol. Opt. Phys. **55**, 034002 (2022).